51st AIAA Aerospace Sciences Meeting including the New Horizons Forum and Aerospace Exposition
07 - 10 January 2013, Grapevine (Dallas/Ft. Worth Region), Texas

AIAA 2013-0908

Initial Assessment of Mars Science Laboratory Heatshield Instrumentation and Flight Data

Deepak Bose*
NASA Ames Research Center, Moffett Field, CA 94035, USA

Todd White†
ERC, Inc., Moffett Field, CA 94035, USA

Jose A. Santos‡
Sierra Lobo, Inc., Moffett Field, CA 94035, USA

Jay Feldman#
ERC, Inc., Moffett Field, CA 94035, USA

Milad Mahzari§
Georgia Institute of Technology, Atlanta, GA 30332, USA

Michael Olson[1] and Bernie Laub[2]
NASA Ames Research Center, Moffett Field, CA 94035, USA

Abstract

The Mars Science Laboratory (MSL) Entry Descent and Landing Instrumentation (MEDLI) suite on MSL entry vehicle heatshield has successfully returned pressure, temperature, and thermal protection system (TPS) ablation data acquired during entry. This paper provides an initial assessment of MEDLI thermal instrumentation data that is comprised of in-depth temperatures in the TPS made of Phenolic-Impregnated Carbon Ablator (PICA). Temperatures are measured in-depth at seven different locations on the surface. The thermal sensor plugs are also characterized in arc jet facilities to quantify measurement uncertainties and biases. The assessment of flight data provides key insights into boundary layer transition to turbulence, surface recession, turbulent heating augmentation, stagnation point and apex laminar heating, and in-depth thermal response. A preliminary comparison with model results highlights inadequacies in our predictive capability. The peak temperature measured by near surface thermocouples was found to be 1049 C in the vicinity of apex region. Initial estimate of peak surface temperature with nominal model settings is about 1575 C. The peak heat flux was found to be on the leeside of the vehicle as predicted, but its value is sensitive to the recession model.

*Aerospace Engineer, AIAA Associate Fellow, Email: Deepak.Bose@nasa.gov
†Research Scientist, AIAA Member
‡ Mechanical Engineer, AIAA Member
# Materials Engineer, AIAA Member
§Graduate Research Assistant, AIAA Student Member
[1]Materials Engineer
[2]Senior Aerospace Engineer, AIAA Fellow

I. Introduction

On August 5, 2012 (Pacific Daylight Time) NASA's Mars Science Laboratory (MSL) entry vehicle entered the atmosphere of Mars at 5.9 km/s and successfully performed an unprecedented entry, descent, and landing (EDL) sequence to land an automobile-sized rover, *Curiosity*, on the surface. The landing of a 900 kg rover, the heaviest payload ever landed on Mars, safely on the ground within a few miles of the target site, represented a significant advancement in NASA's planetary EDL capability. The MSL entry vehicle employed the largest aeroshell [see Fig. 1(a)] on Mars, flew a guided hypersonic trajectory using bank angle maneuvers, deployed a 16 m diameter supersonic parachute, and used an innovative sky crane for touchdown [1].

For hypersonic entry, the MSL entry vehicle was designed to withstand high heating rates > 200 W/cm^2, higher than past Mars entry missions [2,3]. The heritage heatshield material, SLA-561V, used in all past US Mars entry vehicles, was deemed inadequate at such a high heat flux. A new tiled heatshield architecture [see Fig. 1(b)] made with PICA (Phenolic-Impregnated Carbon Ablator) was developed to meet the mission requirements [4].

Despite the significant achievements demonstrated by MSL entry, further developments in EDL technologies are needed before human scale payloads with tens of metric tons of mass can be safely landed on Mars with desired precision and with greater access to higher altitudes. Recently, NASA's Mars Design Reference Mission-5 [5], EDL-Systems Analysis [6] studies and NASA's Technology Roadmap on EDL [7] outlined a suite of mission architectures and technologies that must be developed in order to accomplish the above goals. Many of these candidate technologies require entry using a larger vehicle, flying at higher speeds, and using flexible TPS for deployable systems with lower temperature capability.

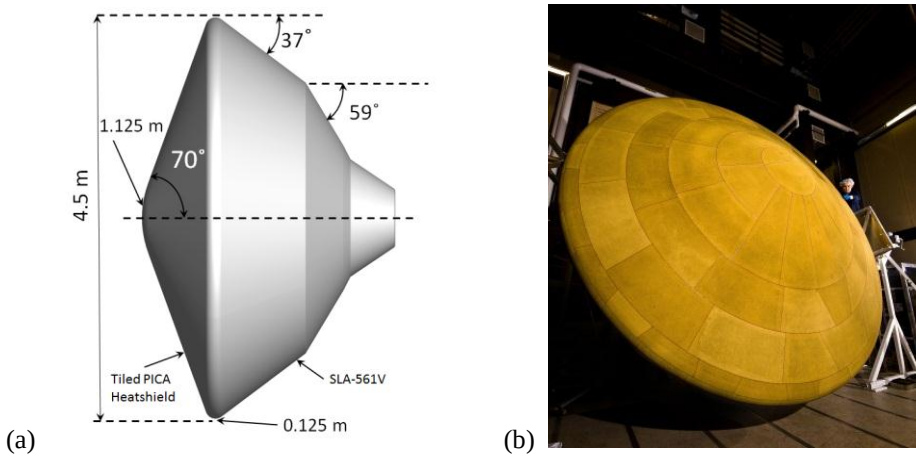

Figure 1. (a) MSL entry vehicle and (b) MSL heatshield made with PICA titles (photo credit: Lockheed Martin Space Systems)

It is also widely recognized that a parallel advancement of predictive modeling capabilities and design tools in aerothermodynamics and TPS response are also necessary to support the technology development goals. As the vehicle size, shape, entry speed, and ballistic coefficient change, so do the critical aeroheating phenomena. For example, as the vehicle size increases and the ballistic coefficient decreases, as in the case of inflatable and deployable systems, the aerothermal phenomena such as boundary layer transition, turbulent heating augmentation, and nonequilibrium radiative heating become critical. Also, with increasing entry speed, catalytic heating due to recombination of dissociated species becomes even more important than it was in previous Mars missions. The state-of-the-art in high enthalpy Mars entry aerothermodynamics is still relatively immature, and prediction uncertainty is as high as 60% for laminar

convective heating [8-10]. While past Mars entry missions with smaller vehicles and/or lower entry speeds have been able to absorb these margins, application of large margins will become difficult in cases where new flexible TPS materials are being developed whose temperature limits are not as high as rigid ablators. Excessive margins will also adversely impact material selection, its testing and qualification requirements, and eventually increase technology development costs. Also, eliminating inherent conservatism in aerothermodynamic models would lead to more efficient designs, higher system performance, and additional payload mass.

With the above mentioned objectives in mind, NASA's MSL heatshield was instrumented to acquire critical data for aerodynamics, aerothermodynamics, and thermal protection system response [11]. The instrumentation suite is called Mars Science Laboratory Entry, Descent, and Landing Instrumentation (MEDLI). The MEDLI suite, consisting of 7 pressure transducers, 24 thermocouples, and 6 ablation sensors, represents the most extensively instrumented Mars entry heatshield. Heatshield instrumentation in past Mars entry missions has been minimal. Viking entry vehicle included two backshell thermocouples, one of which malfunctioned prior to peak heating [12]. Mars Pathfinder had 9 in-depth thermocouples in the TPS and many of them failed to return useable data [13,14]. MSL provided the first opportunity, due to its large aeroshell and high ballistic coefficient, to measure laminar to turbulent transition leading to high heat fluxes during entry into Mars. The MEDLI instrumentation suite performed successfully and returned pressure, in-depth temperatures, and ablator performance data. The dataset is being used to reconstruct vehicle aerodynamics, aerothermal environment, and TPS response during entry. This paper will present the initial assessment of the thermal and ablation data received, and perform some preliminary comparisons with model predictions.

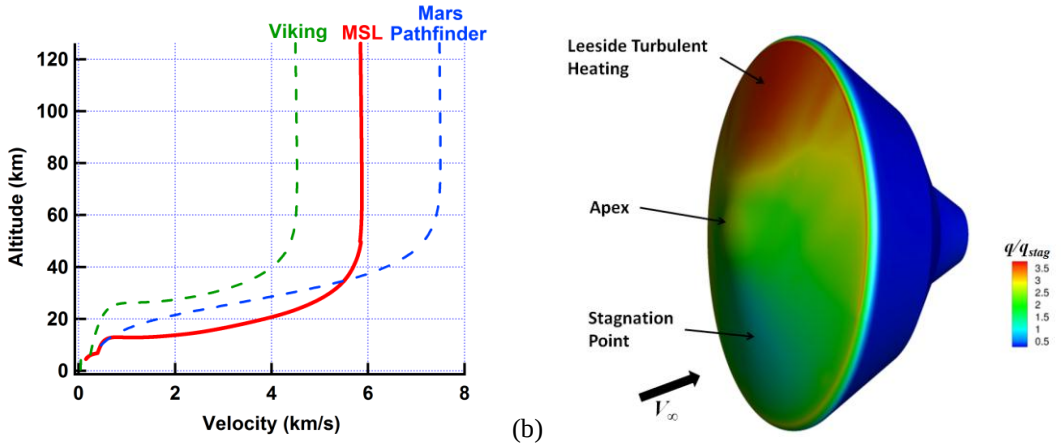

(a) (b)

Figure 2 (a) MSL altitude versus velocity trajectory as compared to Viking and Pathfinder missions (b) Aeroheating map on MSL entry vehicle

It is anticipated that the MEDLI data will form the basis for development of the next generation Mars entry aerothermodynamics models. While grounds tests have driven the development of Mars entry aerothermal and TPS response models thus far, it is widely recognized that ground facilities have significant shortcomings in reproducing relevant flight environments [15,16]. Inadequate model validation in flight has resulted in poor confidence in predicted loads and has required the use of substantial margins [2,3]. In MSL design it is estimated that use of various implicit conservatism and explicit margins increased the required TPS thickness by ~40% over that required with nominal model predictions on maximum heat load dispersed trajectory [3]. For example a substantial recession margin was used to account for a large discrepancy between measured recession in shear environment in the arc jet facilities and the predicted value [17]. It is believed that deficiencies in the test environment and insurmountable limitations of test design are primary causes of this large discrepancy. Validation and calibration of models against flight data are, therefore, essential steps toward developing a robust predictive capability with reduced uncertainty and margins.

II. Mars Science Laboratory (MSL) Entry

The entry trajectory of the MSL entry vehicle is shown in Fig. 2(a) along with two prior Mars missions: Viking and Pathfinder. The MSL entry vehicle flew a guided hypersonic trajectory with a nominal lift-to-drag ratio of 0.24 at a nominal angle of attack of 16-deg. The angle of attack moves the stagnation point away from the center of the vehicle and allows for a large running length on the aeroshell, increasing the possibility of transition to turbulence on the forebody-leeside of the vehicle as seen in Fig. 2(b). In addition, the MSL entry vehicle flew a large aeroshell on a high ballistic coefficient trajectory reaching high flow Reynolds numbers, which ensured transition to turbulence. Past Mars entry vehicles did not experience turbulent heating until after the peak heating point, and as a result were subjected to lower aeroheating.

As the vehicle entered the Martian atmosphere at 5.9 km/s, it was subjected to laminar heating. The freestream enthalpy of 18 MJ/kg was sufficient to dissociate CO_2 into CO molecule and O atoms behind the bow shock wave. The shock layer was expected to be in thermochemical nonequilibrium with temperatures as high as 4000 K. Under these conditions as the reactive species from the shock layer are transported across the boundary layer to the surface, they recombine into CO_2 or react with charred surface and pyrolysis gases injected from the ablator. These recombination reactions cause further heating of the vehicle. The laminar heating is predicted to be highest at the apex of the sphere-cone where the flow turns on a 1.125 m radius spherical surface.

During the entry heat pulse, the TPS begins to pyrolyze forming volatile products that are blown into the boundary layer, leaving behind a charred surface. The pyrolysis gas blowing provides some transpiration cooling, although the dominant cooling mechanism is re-radiation from the high temperature charred surface, which is expected to reach as high as 1600 C. The charred TPS also recedes as it loses material via surface oxidation. During recession, the surface develops roughness features; both distributed roughness due to charring and isolated roughness due to differential recession between PICA and tile gap fillers. These surface roughness features may accelerate boundary layer transition to turbulence.

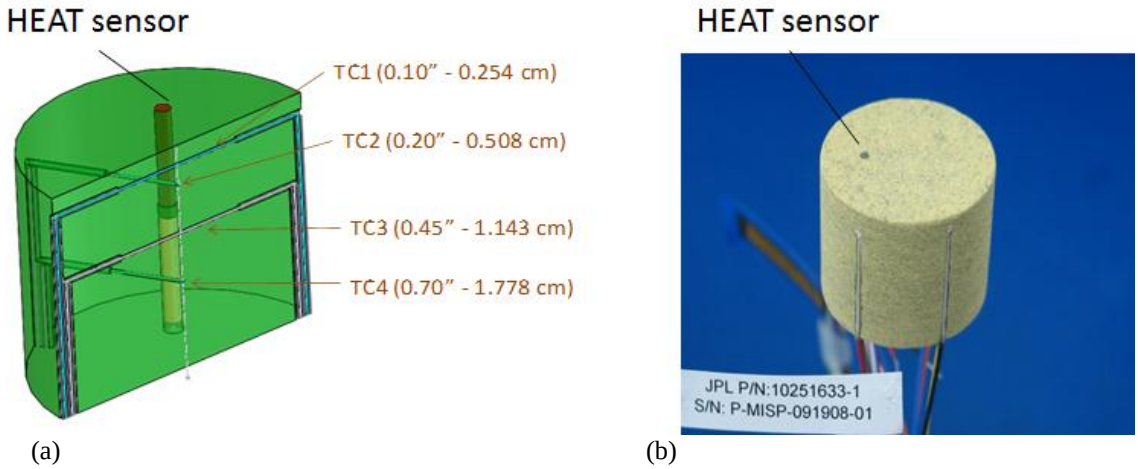

(a) (b)

Figure 3 (a) Schematic of a MISP plug with four Type-K thermocouples and a HEAT sensor (b) MISP plug made with PICA

III. MEDLI Instrumentation, Layout, and Operation

The MEDLI instrumentation suite comprises of two classes of sensors: one for surface pressure measurements called Mars Entry Atmospheric Data System (MEADS) and a second suite of instrumentation for thermal performance (temperature and charring) of the heat shield called the MEDLI Integrated Sensor Plug (MISP). Reference [18] describes the use of MEADS pressure data for

reconstruction of vehicle aerodynamics and atmospheric properties. This paper and Ref. [19] cover the initial analysis of MISP data for reconstruction of aerothermal environments and TPS response.

The MISP instrumentation is embedded in 1.3" diameter and 1.14" deep PICA cylindrical plug. Each MISP plug contained four Type-K (chromel-alumel) thermocouples with 0.012" wire diameter at nominal depths of 0.1, 0.2, 0.45. and 0.7 inch (0.254, 0.508, 1.143, and 1.778 cm) from the initial surface as shown in Figure 3(a) and (b). The top thermocouples are expected to be more responsive to the changes in the surface heating conditions, while the deeper thermocouples are expected to measure in-depth thermal response as heat is conducted through the thickness of the charring, recessing, and pyrolyzing material. In addition to the thermocouples, an ablation sensor, called the HEAT sensor (Hollow aErothermal Ablation and Temperature) [20] is also installed through the thickness as shown in Fig. 4 (a). The HEAT sensor consists of two platinum-tungsten (Pt-W) wires wound around a hollow Kapton, a polyimide insulator, tube; the hollow core is filled with the same Thermal Protection System (TPS) material in which the sensor is installed. As the sensor is heated, the Kapton tube chars and becomes electrically conductive. This conductive path shorts the wires at the char front whose location can be detected by a resistance measurement. The HEAT sensor is shown to follow the time progression of an isotherm through the thickness of the TPS as the material is heated during atmospheric entry. The isotherm temperature which the HEAT sensor follows corresponds to the temperature at which the Kapton has sufficiently charred to establish a conductive path between the two Pt-W wires.

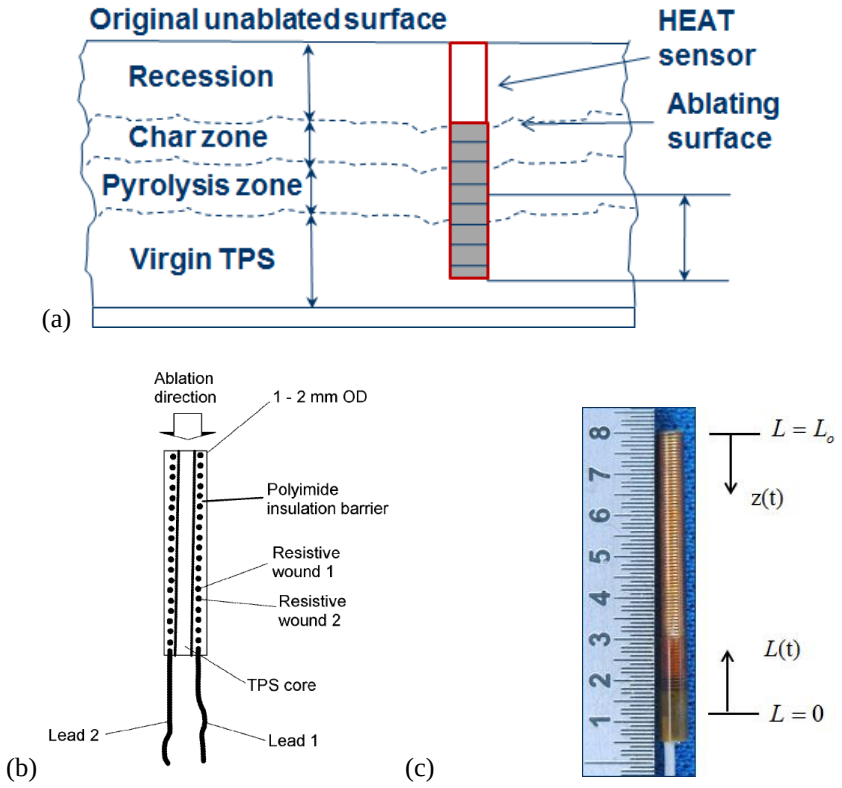

Figure 4 (a) Schematic of a HEAT sensor installed in an ablator, (b) schematic of a HEAT sensor, and (c) HEAT sensor fabricated for MISP plugs

A total of seven MISP plugs are installed on the heat shield. The layout of the plugs is shown in Fig. 5. Each plug is installed on the heatshield using the RTV-560 silicone-elastomer bonding agent as shown in Fig. 6 (a). Figure 6 (b) shows the installation of MEDLI interfaces on the inner side of the heatshield and Fig. 6 (c) shows the tiled MSL heatshield with MISP plugs installed. The plugs are numbered as follows. MISP 1 & 4 are installed in the stagnation region of the forebody while MISP 5 & 7 are embedded in the apex region to capture maximum laminar heating. MISP 2,3, & 6 are located in the leeside forebody to

capture turbulent heating levels, as this region is expected to experience maximum heat flux. No plugs are installed in the backshell of the vehicle. The plugs are arranged along or near the line of symmetry to capture the development and progression of the transition font along the center streamline. MISP 2 & 3 are installed slightly away from the centerline to assess asymmetric heating due to any side-slip angle.

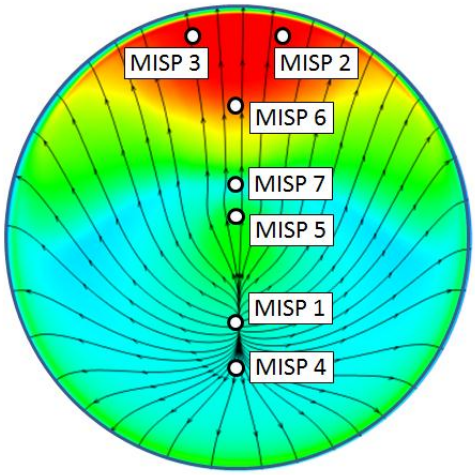

Figure 5 MISP plug layout on MSL heatshield

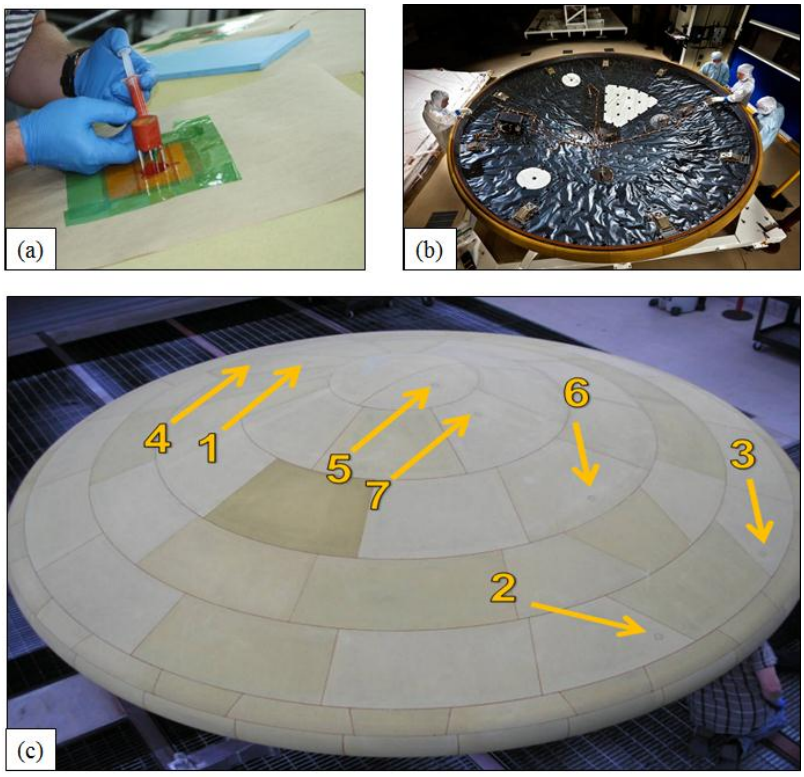

Figure 6 (a) Installation of a MISP plug with RTV-560 bonding agent, (b) MEDLI interface on the inner side of the heatshield, and (c) seven installed MISP plugs on MSL PICA heatshield.

The MEDLI system, that includes MEADS and MISP instrumentation, and the System Support Electronics box, was turned on five hours before entry on August 5th, 2012. The cruise temperatures were found to be

within reasonable limits. Ten minutes before entry MEDLI began to acquire data. The MEDLI timeline is shown in Fig. 7. A subset of the critical MEDLI data was transmitted real time during EDL including tones to indicate incremental progression of events. The full MEDLI dataset was stored in the Rover Compute Element (RCE) for transmission to earth at a later time. The data sampling rate varied from 1-8Hz depending on the sensor. The full dataset was successfully received on earth a few days after landing.

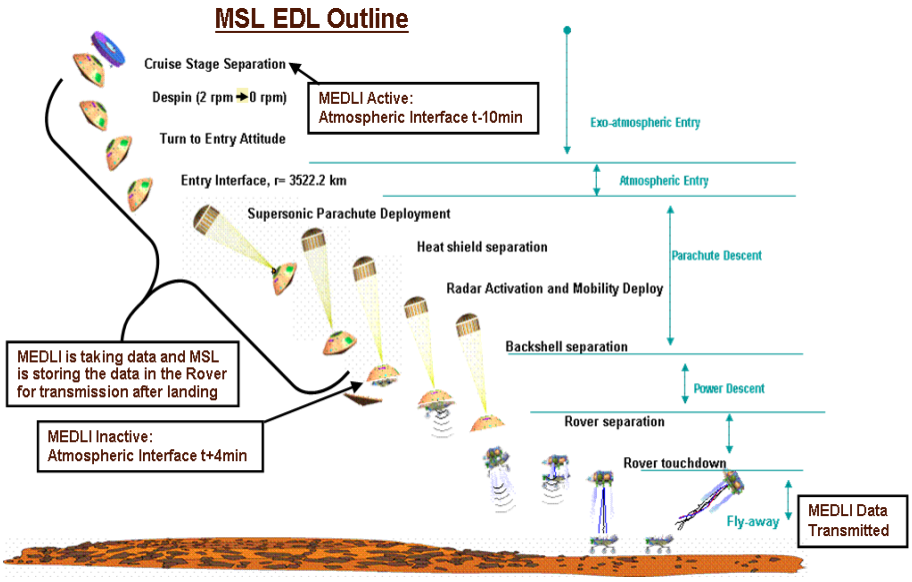

Figure 7 MEDLI timeline during EDL

IV. MISP Science Objectives

The existing uncertainty in Mars entry aerothermal and TPS response modeling for PICA is discussed in Refs. [2,3]. These references also outline pre-flight predictions and margins used for MSL TPS sizing. Much of the uncertainty in modeling is due to a lack of adequate validation data from ground testing. The flight data obtained from MEDLI instrumentation suite will address many outstanding questions that cannot be addressed by ground testing in existing facilities. A set of science objectives listed below have been formulated for the MEDLI-MISP instrumentation suite with the intent to reduce or improve some of the existing uncertainties.

1) *Reconstruct Aeroheating:* Construct the best estimate of the surface heating environment during hypersonic entry
2) *Determine Leeside Turbulent Heating Levels and Augmentation:* Using aeroheating reconstruction, determine turbulent heating levels and roughness augmentation in the leeside forebody of the vehicle to validate CFD predictions and correction factors
3) *Determine Boundary Layer Transition Onset:* Identify time of boundary layer transition to turbulence for validation of transition models and correlations
4) *Determine Stagnation Point Heating Augmentation:* Confirm or reject the presence of augmented heating at the stagnation point that is observed in several wind tunnel measurements
5) *Measure Sub-Surface Material Temperature Response:* Provide in-depth temperature measurements for material response model validation
6) *Determine Total TPS Recession:* Determine total recession of the PICA during hypersonic entry and validate recession model (confirm or reject fail margin)
7) *Measure Depth of Isotherm in TPS:* Using HEAT (isotherm) sensor data to provide isotherm temperature and isotherm depth versus time during hypersonic entry

The post-flight analysis, sensor characterization, tests, and measurements are formulated to meet these objectives, as discussed in the remainder of this paper.

V. Nominal Aerothermal and TPS Response Predictions

The best estimated trajectory for MSL entry based on the flight inertial measurement unit and MEADS data was not available for this initial assessment. A pre-flight estimated trajectory based on the latest orbital determination, OD229, was used in this paper. The altitude versus velocity for this trajectory is shown in Fig. 2(a). This trajectory has been compared with recent best estimated trajectory and there is good agreement between the two during hypersonic phase.

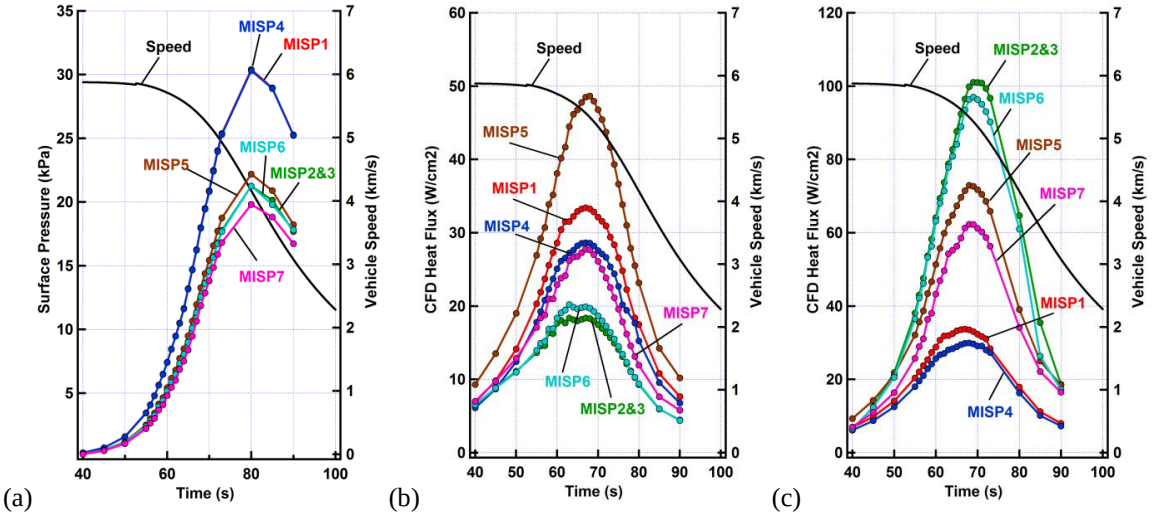

Figure 8 CFD predicted (a) pressure, (b) laminar heat flux, and (c) turbulent heat flux on seven MISP plug locations during MSL entry. Vehicle speed is also plotted for reference.

Our nominal aerothermal and TPS response predictions are made using DPLR [21] and FIAT [22] codes. DPLR is a modern, parallel, structured non-equilibrium CFD code developed at NASA Ames Research Center. The code employs a modified Steger-Warming flux-splitting scheme for higher-order differencing of the inviscid fluxes, and is run here with 2nd order spatial accuracy and to steady-state 1st order in time. For nominal predictions, the flow around the heatshield is modeled as thermochemical non-equilibrium flow, using the Mitcheltree and Gnoffo [23] 8-species (CO_2, CO, N_2, O_2, NO, C, N, and O) Mars model. The Mars atmosphere is modeled as 97% CO_2 and 3% N_2 by mass. The TPS surface is modeled as an unblown, non-slip, radiative equilibrium wall with constant emissivity ($\varepsilon = 0.85$) and the Mitcheltree and Gnoffo surface catalycity model. Species diffusion is modeled using self-consistent effective binary diffusion (SCEBD). Turbulent flow is simulated with the Baldwin-Lomax algebraic model. CFD calculations are performed along the entry trajectory, at 2-5 second intervals. Surface properties for material response simulations are extracted from the CFD solutions at each MISP location. These quantities are then fitted in time with tight monotonic cubic splines, and provided as inputs to the FIAT material response code at quarter-second intervals.

Figure 8 shows nominal pressure, laminar heat flux, and turbulent heat flux predictions from CFD at the seven MISP plugs during entry. Figure 9 shows FIAT predicted through-the-thickness temperature, TPS recession front, and char front due to pyrolysis and surface oxidation of the PICA ablator during entry at the MISP locations. For TPS response modeling the aerothermal environment is switched from laminar to turbulence as local momentum thickness Reynolds number, Re_θ reaches 200. It is worth noting that a constant 1.25" (31.75 mm) thick TPS was used on the vehicle which should be compared to the depths in Fig. 9.

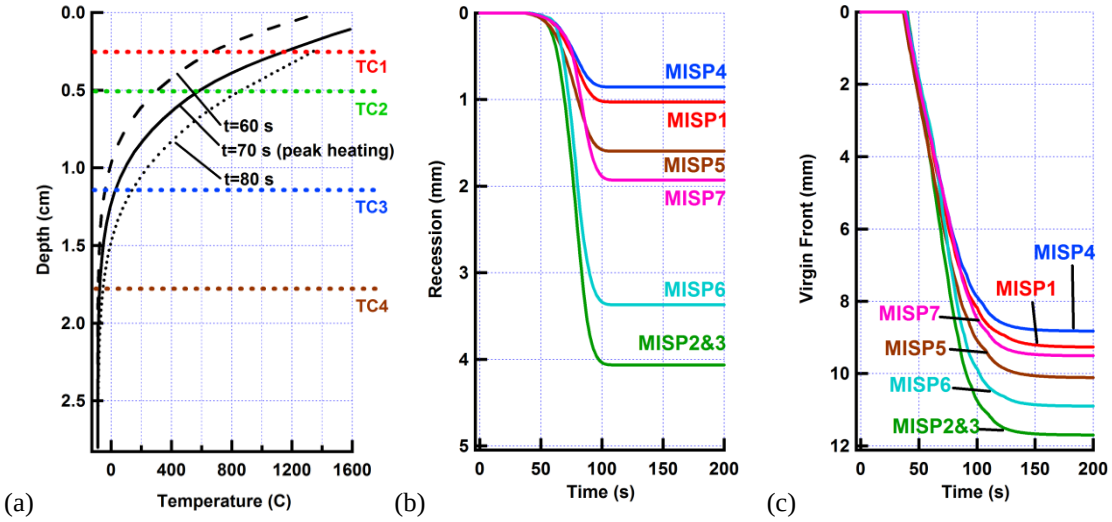

Figure 9 FIAT predicted (a) in-depth temperatures at different times during entry at MISP2&3 locations, (b) recession front, and (c) virgin front at all MISP plugs.

VI. MISP Sensor Testing, Measurements, and Calibration

A. Instrumentation Error Budget

In order meet the science objectives of the MISP subsystem, measurement errors, biases, and uncertainties in instrumentation must be quantified. An assessment of various instrumentation errors and sources of uncertainty are being made based on various data sources from manufacturing, installation, laboratory tests, arc jet tests, simulations, and literature review. A detailed itemized quantification and substantiation of various errors are provided in Ref. [24]. For MISP thermocouples, accuracy of EMF output, impact of thermal gradients, chemical interactions, thermal lag and perturbation, electrical shunting, bead location, etc. have been considered. For MISP HEAT sensors, uncertainties such as resistance measurement, sensed depth, thermal gradient correction, and inferred isotherm temperature have been considered. In this paper we discuss only some of these errors that have significant impact, and provide a current status of sensor error investigations. The test and analysis are on-going, and the results will be presented in future publications.

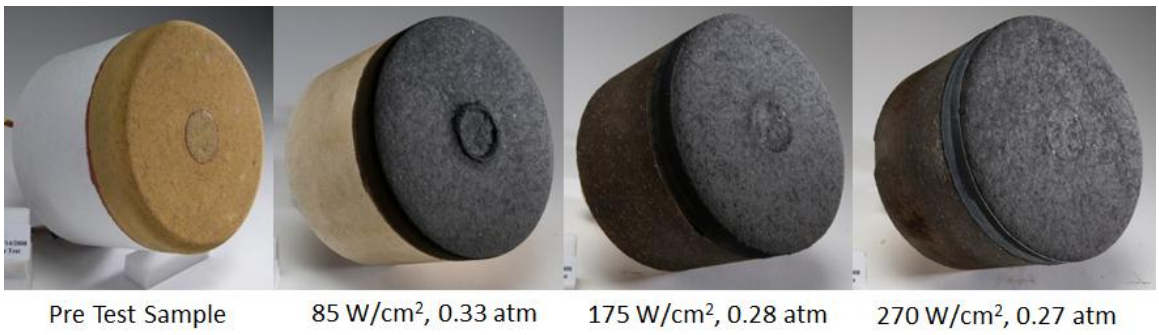

Figure 10 RTV "fencing" caused at low heat flux conditions

1) HEAT Sensor Isotherm: The sensed depth of a HEAT sensor represents the depth where Kapton, a polyimide-insulator which encapsulates the sensor wires, becomes sufficiently charred to form an electrical contact. This moving char front represents a constant temperature isotherm. Prior thermo-gravimetric analysis and furnace tests have provided an initial estimate of this temperature

[25]. A set of arc jet tests are performed to estimate the measured temperature isotherm in a flight relevant environment with the HEAT sensor installed in MISP hardware. Laboratory testing shows that the isotherm represented by the HEAT sensor depends on the heat rate (temperature rise rate). The test results and inferred isotherms at flight relevant heat rates are also discussed in the next section.

2) Thermal Lag: A thermal lag due to a 0.012" Type-K thermocouple wire embedded in a low density ablator arises because of the finite thermal mass of the thermocouple. A finite thermal mass contributes to a slower response and a perturbation of the temperature field. The thermal lag is being quantified by testing arc jet models with standard MISP plugs that have additional instrumentation of fast-responding SMART thermocouples [26]. Two SMART Type-K thermocouples, made with thinner 0.001" wire are installed in each plug at the same depth as the top two 0.012" MISP Type-K thermocouples. A direct comparison between 0.012" Type-K and 0.001" Type-K wire at flight relevant heat fluxes provides a measure of the effect of thermal mass on thermal lag. The results of the tests are discussed in the next section.
3) RTV Fencing: RTV-560 is a silicone-elastomer used for high temperature bonding. At flight relevant temperatures the compound forms a glass melt layer that swells over the ablator surface and forms a "fence" around the plug. This fencing phenomenon is seen in post arc jet tested samples that are subjected to low (but flight relevant) heat fluxes (< 100 W/cm^2). Some examples of fencing are shown in Fig. 10; the fencing occurs on both stagnation and shear test articles. At higher heat flux, the fencing is minimal presumably because of a faster material removal that prevents any RTV swelling to rise above the surrounding PICA surface. The protrusion of these features into the boundary layer can cause perturbation of heating at the plug as well as in the downstream regions. The disturbance in the boundary layer can also grow, and if suitable conditions persist it can induce transition to turbulence. A secondary effect of silica coverage on plug surface from RTV melt is also seen in low heat flux shear tests. An excessive surface coverage can alter surface emissivity with an impact on surface temperature. Arc jet testing was recently performed to quantify the effect of RTV on in-depth thermal response. The results of the tests are presented in the next section.

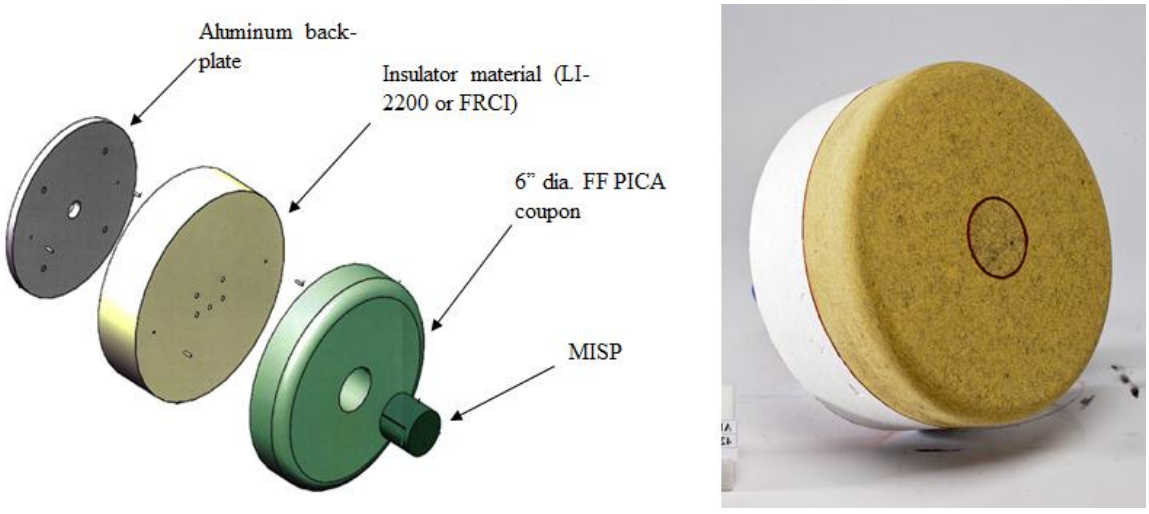

(a) (b)

Figure 11 Arc jet test model for stagnation testing (a) material stack up and (b) a 6" flat-faced PICA model with a MISP plug bonded with RTV-560.

B. Arc Jet Testing

Arc jet testing is done to characterize the performance of the MISP sensor in a flight-like environment. The following major objectives are identified for the test campaign.

1) Determine HEAT sensor isotherm and its uncertainty

2) Quantify thermal lag due to the use of 0.012" Type-K thermocouple wire
3) Quantify RTV fence height and its impact on in-depth thermocouple reading

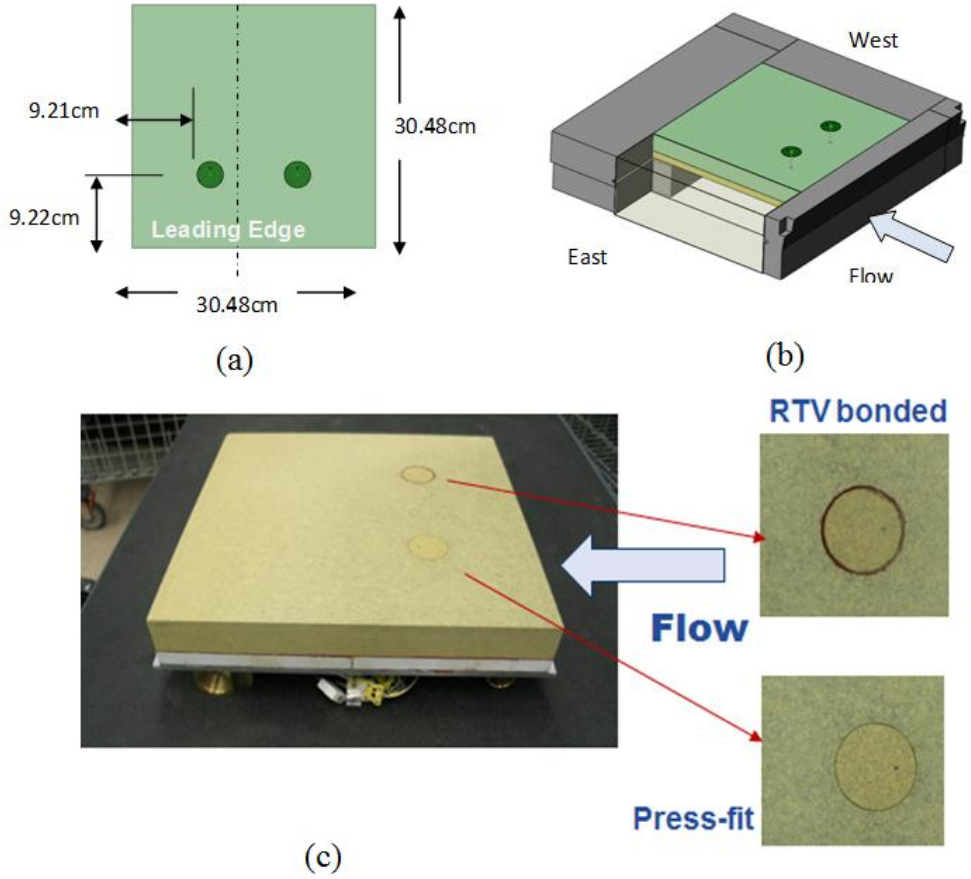

Figure 12 Arc jet test model for shear testing (a) panel dimensions and MISP plug placement (b) schematic of the panel holder, and (c) a PICA panel with two MISP plugs installed; one with RTV bonded and one press fit into the panel.

MISP plugs, identical to the flight plugs, are installed in 6-in. diameter PICA coupons for stagnation testing and in 30.48 cm square PICA panels for shear testing. Figures 11 and 12 show the model design for stagnation and shear testing respectively. The test coupons, panels, and the MISP plugs are fabricated using the same billet of PICA that was used to manufacture the flight plugs. This ensures consistency in material properties and reduces the variability that exists between different billets. The arc jet test conditions are chosen to match the predicted flight environment, especially heat flux and enthalpy. However, given the limited flexibility in model size and facility operating conditions, a full sweep of the flight conditions at all MISP locations was not possible. The facilities in the NASA Ames Arc Jet Test Complex are used for testing. For stagnation testing the Aerodynamic Heating Facility (AHF) and Interaction Heating Facility (IHF) are being used. All tests are conducted with air mixed with some Ar as the working gas. The capability to test in a CO_2 atmosphere is not available at this time, although it is not considered critical to meet the test objectives. The Ames Panel Test Facility (PTF) is used for shear testing. For testing in turbulent flow conditions, Ames Turbulent Flow Duct (TFD) will be used. Figure 13 shows the arc jet test conditions and their relevance to flight environments. In this paper we discuss the key results obtained from the tests thus far. The results and conclusions are subject to refinement as we complete the test program.

1. HEAT Sensor Isotherm

The HEAT sensor was tested at heat fluxes between 15-80 W/cm^2 (cold wall). The sensed depth from the HEAT sensor was compared against in-depth thermocouple measurements to infer an isotherm represented

by the sensor. Figures 14 (a) and (b) simultaneously show the time response of the HEAT sensor (sensed depth) and the in-depth thermocouple readings at 19 W/cm^2 and 67 W/cm^2 (cold wall). As the HEAT sensor depth crosses the thermocouple depth, its temperature is noted as the isotherm temperature. The isotherm temperatures are then collected for different tests and at different HEAT sensor depths. In flight, the predictions show that HEAT sensor depth is unlikely to reach the fourth thermocouple at a depth of 1.8 cm. The isotherm data obtained from tests to date are plotted in Fig. 14 (c). The HEAT sensor follows an isotherm from 760 C-880 C at flight like conditions until the depth of 0.5 cm. The third thermocouple (at 11.43 mm) shows a slightly lower isotherm for the HEAT sensor, but given the scatter in the data, we refrain from making a conclusion until additional data are collected. A complete analysis will be presented in a later publication upon completion of the test program. The scatter of 120 C is reasonable once we consider that accuracy of HEAT depth is 0.7 mm in a region where temperature gradient can be as high as 300 C/mm. Uncertainty due to thermocouple reading also contributes to the scatter.

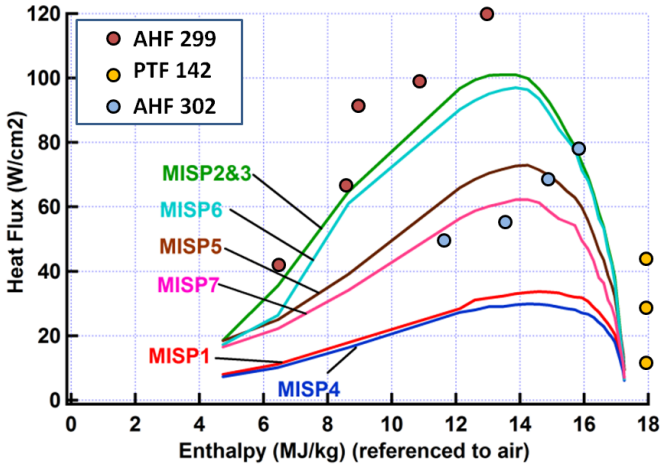

Figure 13 Arc jet test conditions and relevance to flight environment at MISP plug locations

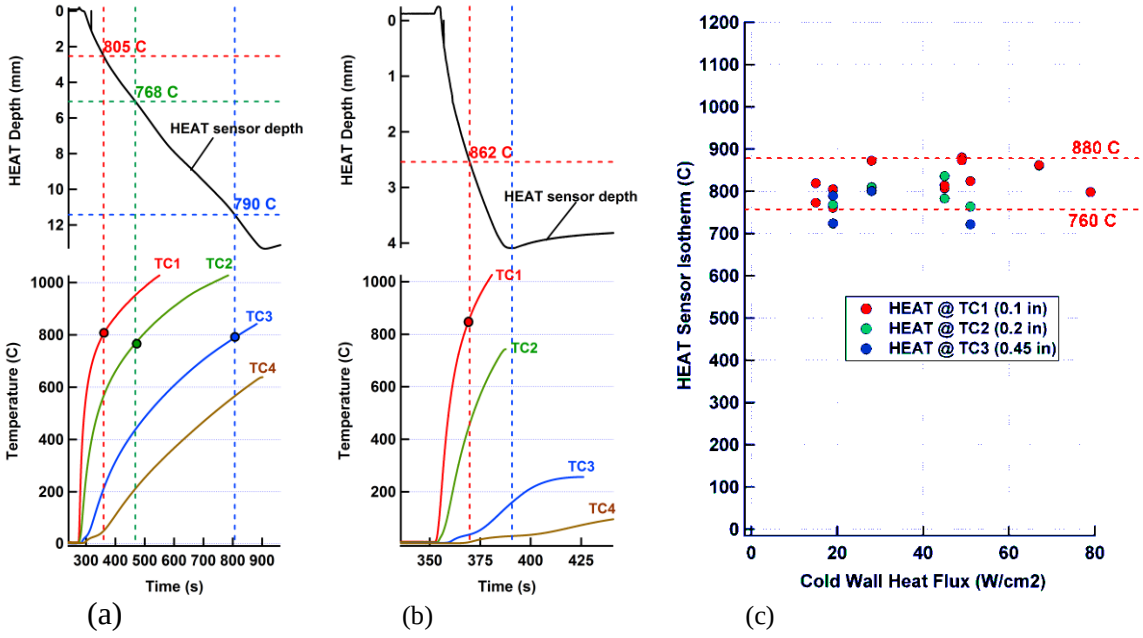

Figure 14 HEAT sensor depth and thermocouple readings from arc jet testing at cold wall heat fluxes of (a) 19 W/cm^2 and (b) 67 W/cm^2. (c) HEAT sensor isotherms inferred at different cold wall heat fluxes.

2. *Thermal Lag*

Thermal lag, caused by the finite thermal mass of the 0.012" Type-K wire, is quantified by comparing its response against fast-responding SMART Type-K thermocouples (0.001" wire) that were installed in the same arc jet model. Figure 15 shows the relative responses of the two thermocouples in the arc jet. A direct comparison shows a thermal lag of 3.5 s at 800 C in the 95 W/cm^2 test and a thermal lag of 1.5 s at 800 C in the 139 W/cm^2 test. The data, however, must be understood in the context of the uncertainty in thermocouple depth. The installation of the MISP and SMART thermocouples are nominally at the same depth, but this can only be ensured via X-ray measurements to within 0.08 mm. As seen in Figure 9, in a region where the thermal gradient is ~300 C/mm, a 0.08 mm distance spans 24 C, which is a large portion of the discrepancy between the thermocouples. Further assessment of this data along with thermal modeling will be undertaken to find a reasonable correction for thermal lag.

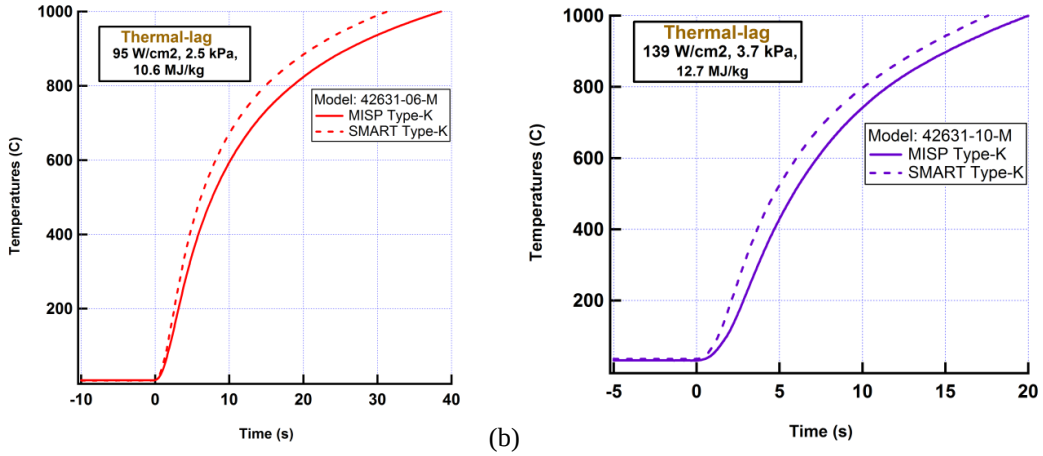

(a) (b)

Figure 15 Comparisons of MISP 0.012" Type-K thermocouple with SMART Type-K thermocouple nominally at 2.54 mm depth in arc jet tests at (a) 95 W/cm^2 and (b) 139 W/cm^2 (cold wall).

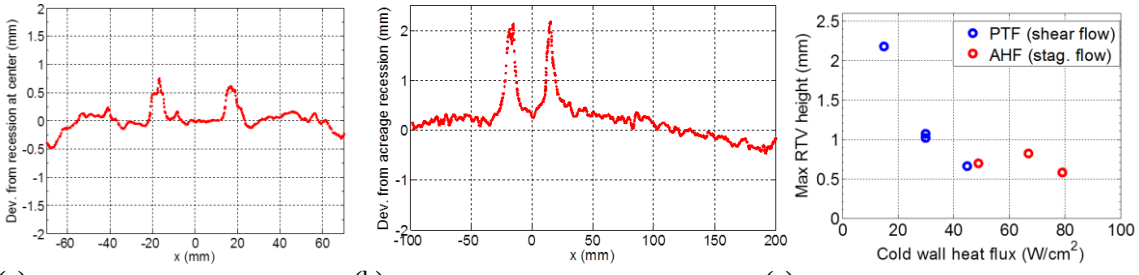

(a) (b) (c)

Figure 16 (a) and (b) Laser profilometer scans of post arc jet tested samples measuring RTV fence height, and (c) correlation of RTV fence height with heat flux.

3. *RTV Fencing*

The effect of RTV fencing is quantified by comparing results from two arc jet models: the first model includes a MISP plug bonded with RTV-560, similar to flight hardware, while in the second model the MISP plug is press fit into the counter bore. Laser profilometer measurements of RTV fencing in post arc jet tested samples show a correlation of fence height with heat flux, a lower heat flux leads to a larger fence height, as shown in Figure 16. Figure 17 shows the comparison of in-depth as well as surface temperatures obtained from stagnation test in the arc jet. The surface temperature is obtained from a two-color pyrometer. In order to minimize arc jet freestream variability, the models are introduced in the stream

consecutively in the same run. The result indicate a lower heating experienced by the plug bonded with RTV, possibly due to a "cavity-effect" caused by the fencing. A similar result is obtained in shear testing where two plugs; one RTV bonded and one press-fit, are exposed to the same arc jet stream. The uniformity of the arc jet stream is confirmed by exposing a control model with two press-fit plugs and verifying a consistent thermal response.

Table I shows the summary of the error budget based on tests and analyses conducted thus far. The individual errors will be refined and a total measurement uncertainty will be estimated in future.

Table 1 Summary of MISP error budget

Category	Description	Estimated Error	Remarks
Thermocouple	Type-K thermocouple wire error	±0.4%	Ref. [24]
	Extension wires and connectors	±0.75%	Ref. [24]
	Electrical Shunting	+0, -2.8%	Ref. [24]
	Bead location	±12 C	Ref. [24]
	Thermal lag	1-3 s	at 20-80 W/cm^2
HEAT Sensor	Isotherm temperature	760-880 C	at 20-80 W/cm^2
	Isotherm depth	0.7 mm	Ref. [24]
Plug Integration	Effect of RTV fencing	assessment on-going	

VII. Flight Data Assessment

A. MISP Data

In this section we discuss the flight data received, the initial assessments, and the on-going analyses to meet the MISP science objectives. A few days subsequent to the successful landing of *Curiosity*, the complete MEDLI dataset was received from the RCE. Channels of raw voltages and currents were converted into thermocouple temperatures and HEAT sensor resistances. All 24 MISP temperatures and 6 HEAT sensor resistances as a function time were received. Four thermocouple traces were obtained for each MISP plug, except plugs 4 and 7 which did not have the two deepest thermocouples wired due to number of channel limitations. Plug 4 did not have the HEAT sensor wired. The as-received MISP temperatures are shown in Fig. 18. All thermocouples returned data successfully that appear to be virtually noise free. The data from the HEAT sensors, however, showed unusual behavior during the heat pulse. The HEAT sensor data is still being assessed for quality and will be presented in future papers. The pressure data from the MEADS pressure transducers were also retuned successfully. The reader is encouraged to refer to Ref. [18] for MEADS pressure data assessment.

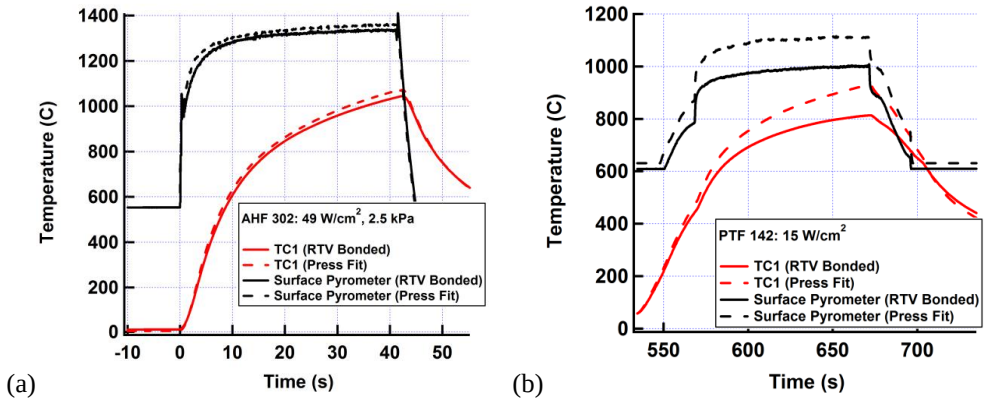

(a) (b)

Figure 17 Surface (from pyrometer) and in-depth temperature comparisons between two MISP plugs: one that is RTV bonded and one press fit. (a) Stagnation test at 49 W/cm^2 (cold wall) and (b) shear test at 15 W/cm^2 (cold wall). TC1 represents a thermocouple at an initial depth of 2.54 mm as shown in Fig. 3(a).

B. Analysis Plan

Although this paper only presents an initial assessment of the MISP flight data, a comprehensive analysis is underway to reconstruct the aerothermal environment and TPS response. The analysis plan includes a direct analysis [27] as well as an Inverse Parameter Estimation (IPE) [19]. In direct analysis, the best estimated flight trajectory is used to generate the aerothermal environment using a CFD code, which is then used as input for a material response code. The predicted in-depth temperatures from the material response code are compared with the flight data for assessment. The IPE on the other hand works in the reverse direction. It uses the MISP temperature data, and by using optimization techniques, built around the material response code, converges on an aerothermal environment that produces the best match with the data. The preliminary results of an inverse analysis are discussed in detail in Ref. [19] and are not discussed further in this paper.

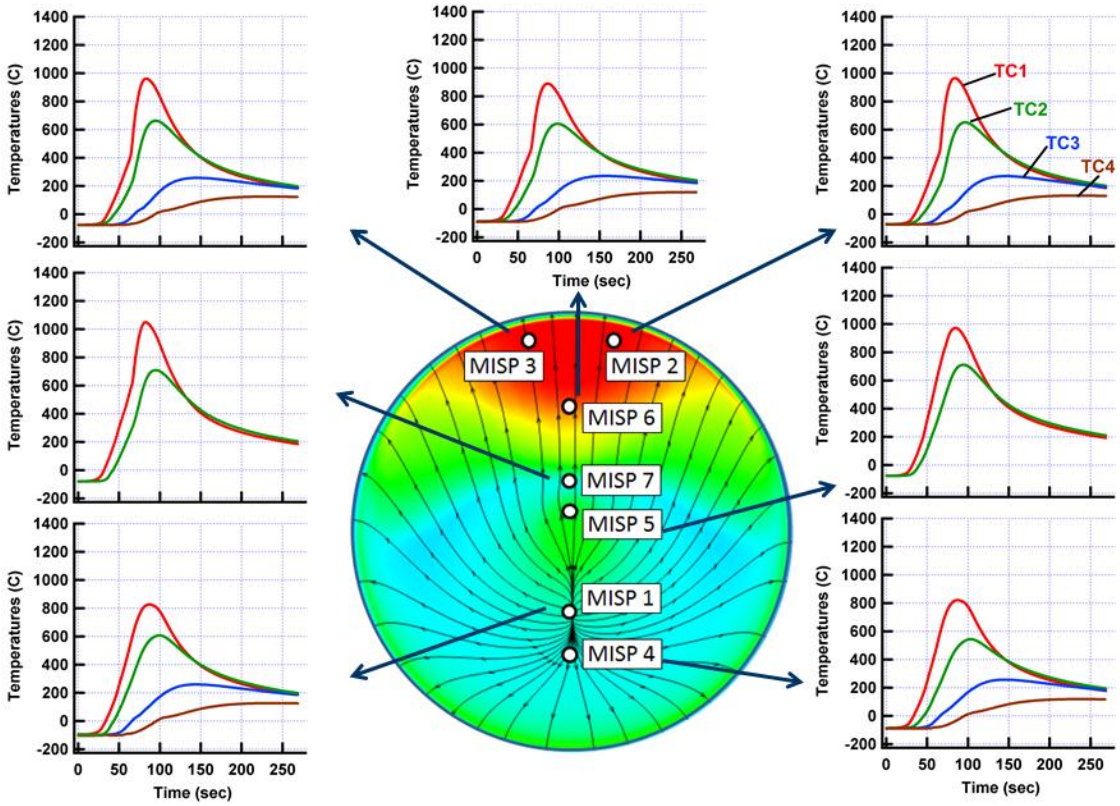

Figure 18 MISP thermocouple data obtained during MSL entry. TC1, TC2, TC3, and TC4 represent thermocouples at nominal depths shown in Fig. 3(a).

C. Boundary Layer Transition

One of the readily noticeable features in the flight thermocouple data is onset of turbulence, which can be identified by a sudden change in the slope of the temperature traces. As flow over the heat shield transitions from laminar to turbulent, the heat flux jumps several fold, which is reflected in the data as an instantaneous change in the rate of temperature rise. The onset of turbulence before peak heating is apparent in all four plugs (2, 3, 6, & 7) on the leeside. The windside plugs do not show onset of turbulence, which is consistent with expectations. The transition to turbulence is most obvious in the top thermocouple traces due to its proximity to the surface; the signal is progressively muted in deeper thermocouples. Figure 19 shows the top thermocouple traces from all seven plugs. A more obvious demonstration of boundary layer transition is seen when temporal slopes of temperature traces are simultaneously plotted for every

plug. It is seen that transition first begins at MISP3 and immediately followed by MISP2, and within one second the transition front reaches upstream to MISP7, as schematically shown in Fig. 19 (d).

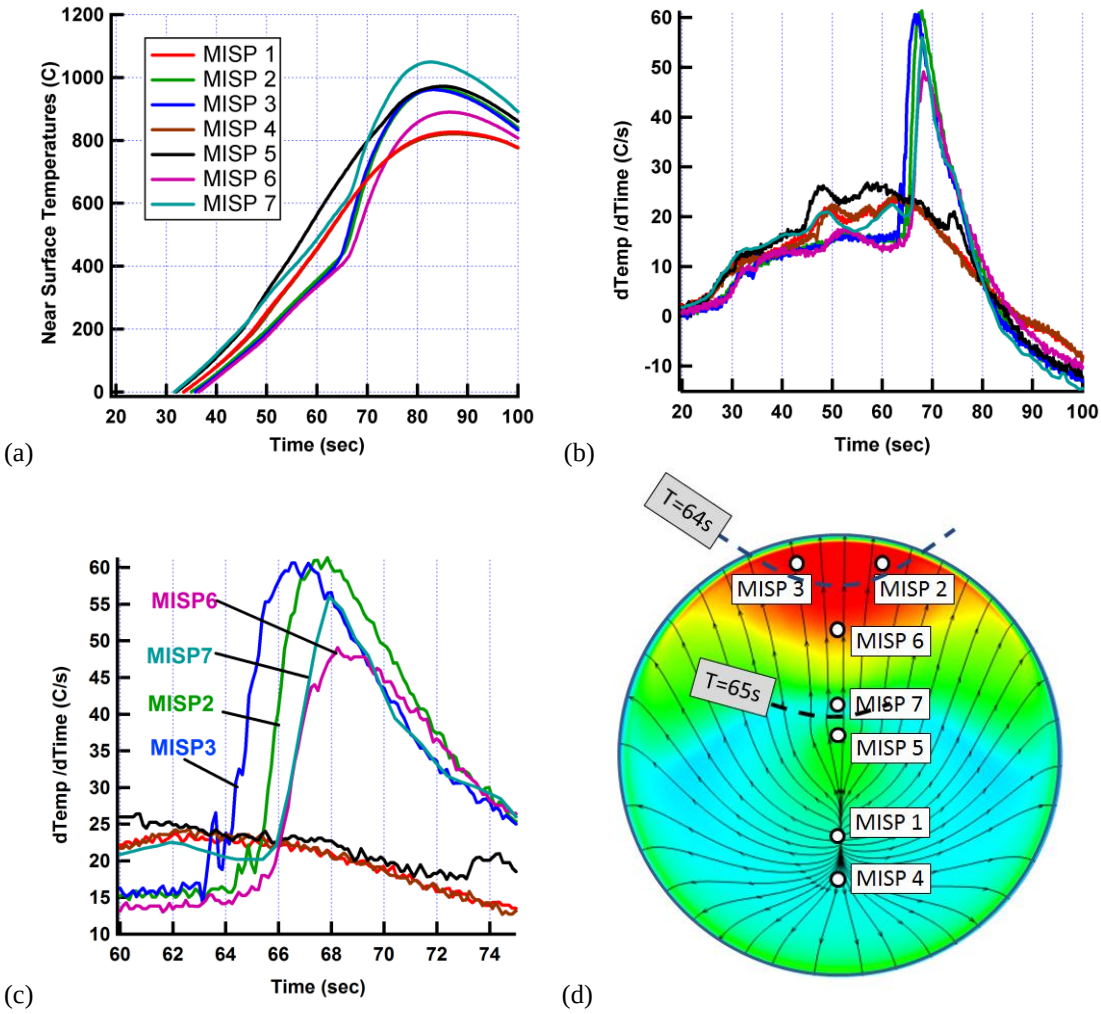

Figure 19 (a) Top thermocouple (2.54 mm deep) data from each MISP plug, (b) temperature-time slope of top thermocouple data, (c) magnified temperature-time slope of top thermocouple data, and (d) notional transition front on the aeroshell.

The prediction of boundary layer transition is generally made using a critical Reynolds number based correlation such as the momentum thickness Reynolds number, Re_θ >200 [28] for smooth surfaces or one of the roughness based transition criteria for Re_{kk} [29], where k is the characteristic roughness height. Figure 20 shows time variation of Re_θ and Re_{kk} based on laminar CFD computations at four leeside plugs. It is seen that Re_θ >200 predicts an earlier transition for MISP2, 3 and 6, but a later transition for MISP7. The Re_θ correlation predicts a slower progression of the transition front forward. The transition times are summarized in Table 2. The roughness based Re_{kk} correlation, however, shows a rapid progression of transition front from MISP2 to MISP7 as observed in the flight data. An assumption of a 2 mm isolated roughness due to RTV fencing is made, as supported by measurements in Fig. 16 (a) and (b). The critical Re_{kk} for transition depends on whether it is caused by isolated roughness (critical value ~600) or distributed roughness (critical value ~250). Figure 20 (b) shows that for a large roughness element (~2 mm), all four MISP plugs on the leeside have very similar Re_{kk} values and will likely experience transition simultaneously. These observations suggest that surface roughness may be the cause of transition. A more thorough analysis is necessary to conclusively demonstrate a cause of transition. The possibility of distributed roughness as a cause of transition must also be explored.

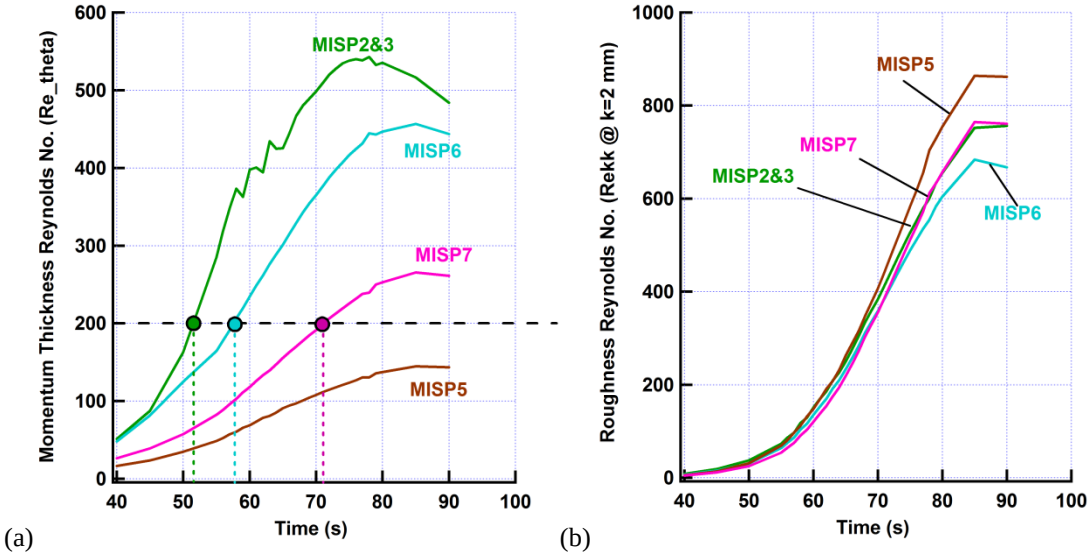

Figure 20 (a) Re_θ and (b) Re_{kk} (with k=2 mm) traces from laminar CFD computations

Table 2: Boundary layer transition times from MISP data compared to predictions from Re_θ >200

Plug	Flight Transition Time (sec)	Predicted Transition Time with Re_θ>200 (sec)
MISP3	63	52
MISP2	64	52
MISP6	65	57
MISP7	65	71

D. Comparisons with Temperature Predictions

Figure 21 shows initial comparisons of as received data with pre-flight predictions. No attempt has been made to reconcile the timing of the boundary layer transition in this initial assessment. The model predictions use Re_θ >200 as the transition criterion, which was used in pre-flight MSL aerothermodynamic assessment [2]. The discussion in this section is divided into three parts: stagnation region (MISP 1&4), apex region (MISP5 & 7), and the leeside region (MISP2,3,&7).

1. *Stagnation Region (MISP1 &4)*

In both plugs the in-depth peak temperatures at the top thermocouple is under predicted by about ~100 C. The under prediction of the peak temperature could be due to a variety of reasons; the most likely cause being a lower prediction of stagnation point heating. A full sensitivity analysis is underway to detect primary factors that could explain this discrepancy. It is unlikely to be due to errors in the flight trajectory used for the CFD since the predictions of pressure versus time shows an excellent match with measurements obtained from the MEADS instrumentation. Other causes such as surface recession, surface emissivity, nonequilibrium surface chemistry, high temperature thermal properties of char, and even presence of radiative heating are being explored. It is worth noting that an under prediction of stagnation point heating is also seen when comparisons are made with wind tunnel data, especially at turbulent conditions [2]. In MSL TPS sizing, a stagnation point heating margin of about 50% was implemented to account for this under prediction. The under prediction of the wind tunnel data has, however, been hypothesized to be due to tunnel related causes such as freestream turbulence or particle impact, etc. In

light of the comparisons with flight data, a re-assessment of our ability to predict stagnation point aeroheating must be made.

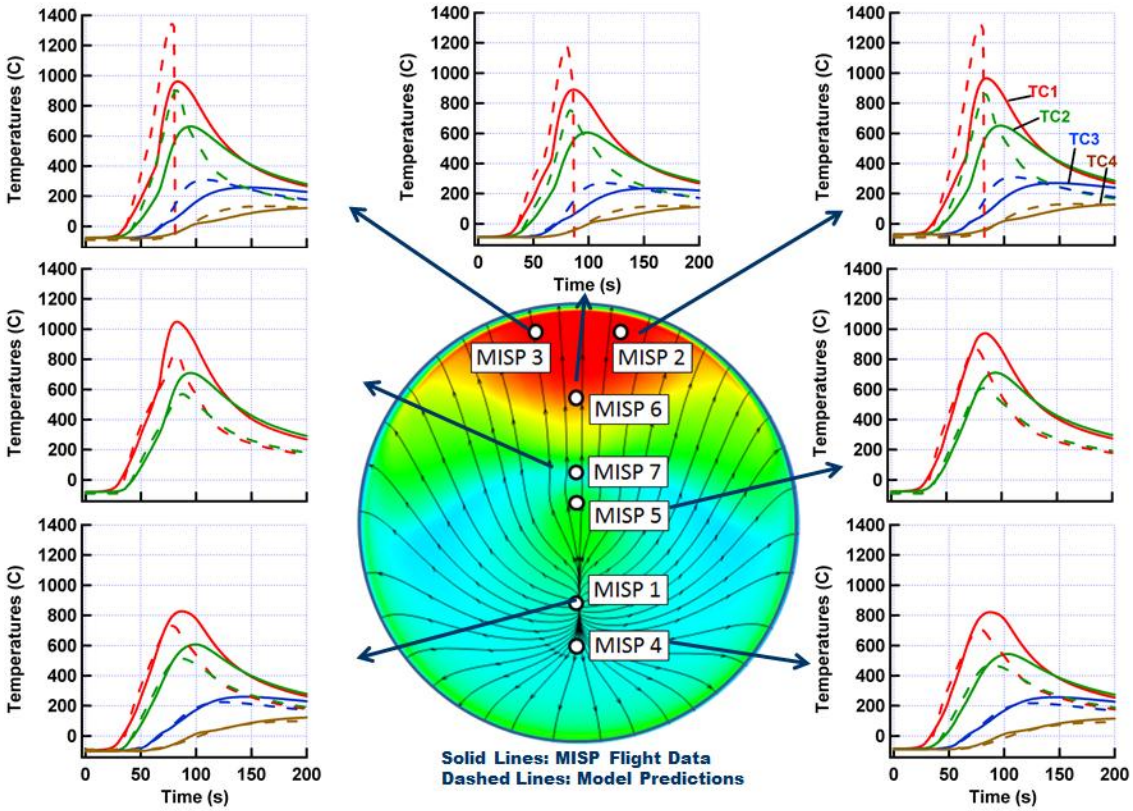

Figure 21 MISP thermocouple data obtained during MSL entry compared with nominal (unmargined) model predictions. TC1, TC2, TC3, and TC4 represent thermocouples at nominal depths shown in Fig. 3(a).

2. *Apex Region (MISP5 &7)*

The laminar heating is the highest in the apex region (see Fig. 8) where the flow turns around a relatively low radius of curvature surface. On MISP5 & 7, similar to the stagnation region, the peak temperatures are under predicted by the models. Some of causes of this discrepancy could be similar to those discussed for stagnation region heating under prediction. At MISP5 the peak predicted temperature is lower by about ~100 C for the top thermocouple, whereas at MISP7 the under prediction is exacerbated by the prediction of a late boundary layer transition as discussed before. The peak temperature at this MISP location is higher by about ~210 C than model predictions. Surprisingly, the highest MISP temperature measured is at MISP7 which has neither the highest laminar nor the higher turbulent heating, although, the vicinity of MISP7 has a large variation of heat flux due to changing radius of the curvature of the surface. An evaluation of heating profiles near the apex region will be made to address this discrepancy.

3. *Leeside Region (MISP2,3 &7)*

The leeside of the vehicle forebody clearly experienced turbulent heating. Initial comparisons of the temperature data shows that, unlike other regions of the heatshield, the predicted peak temperatures are much higher than measurement. In fact, the top thermocouple temperature in model prediction rises until the surface recession front reaches the thermocouple depth, which is nominally 2.54 mm. In flight, however, the recession front does not reach the top thermocouple. Recession and the proximity of the top thermocouple to the ablator surface are critical factors that need to be assessed before reasonable

predictions of the top thermocouple temperatures are made. Due to a high temperature gradient between the top thermocouple and the surface, the distance between the two is a critical factor. The sensitivity of temperature predictions on surface recession is considered in the next section. The other reasons for higher predicted temperatures could be due to early onset of turbulence in the leeside region and a possible deficiency of the turbulence model used. All of above factors will be investigated later via sensitivity analyses.

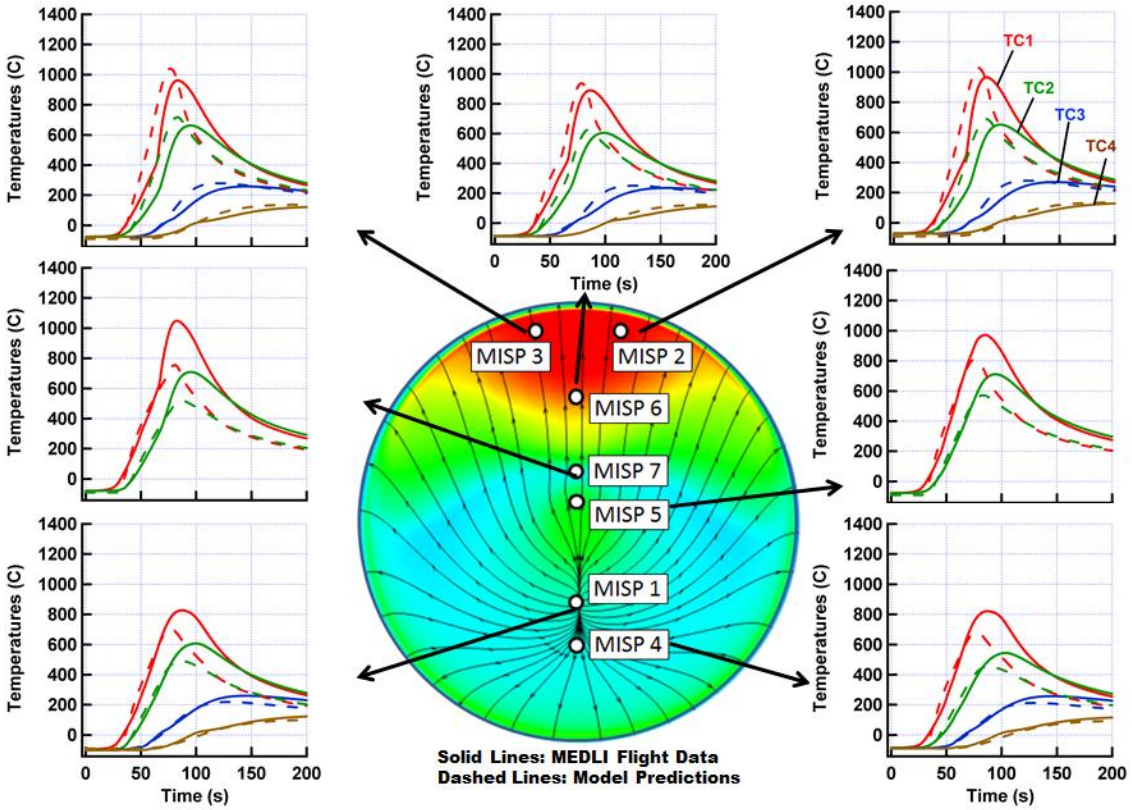

Figure 22 MISP thermocouple data obtained during MSL entry compared with model predictions when surface recession is turned off. TC1, TC2, TC3, and TC4 represent thermocouples at nominal depths shown in Fig. 3(a).

E. Recession Sensitivity

Although the top thermocouple is installed nominally at 2.54 mm (0.1 in) from the surface, recession during entry reduces this distance. This is a critical region through the ablator thickness as the temperature gradient in the top layer of the ablator can be as high as 300 C/mm during peak heating as shown in Fig. 9. The temperature at the top thermocouple is therefore expected to be sensitive to the instantaneous depth of the thermocouple (i.e. recession). It is also known via comparisons with arc jet tests that at low heat flux conditions (< 100 W/cm^2), the TPS response models generally over predict surface recession [30]. This over prediction occurs due to the assumption of thermochemical equilibrium at the surface between boundary layer edge species, the char surface, and the pyrolysis gases. The prediction of atomic oxygen concentration under nonequilibrium conditions at the surface is cited as one of the causes of over prediction of surface recession [30]. The MISP flight data also confirms the over prediction of recession by the models. The survival of all top thermocouples during the entire heat pulse indicates that total surface recession less than 2.54 mm (0.1 in), whereas the models predict a recession as large as 4.1 mm [see Fig. 9 (b)].

In this preliminary assessment we re-ran model predictions with no recession to quantify the bounds of variability in temperature predictions. Figure 22 shows the comparisons when surface recession is turned

off. The model predictions are now closer to the MISP temperatures at the leedside plugs (MISP2, 3 & 6). However, the predictions are slightly worse for MISP7 & 5. The level of comparison is minimally affected in the stagnation region since total recession is low in this region. The intent here is to only show the sensitivity to recession and it is not claimed that recession is non-existent in flight.

VIII. Ongoing Work and Concluding Remarks

The MEDLI-MISP subsystem successfully acquired heatshield temperature data during the MSL entry. All thermocouples returned reasonable data with virtually no noise. The HEAT sensor data are still being evaluated for quality due to the presence of anomalous noise during the heat pulse. The steady state reading of the HEAT sensor is reasonable and will be assessed for char depth evaluations. The initial assessment of MISP temperature data has provided valuable insights and highlighted areas of further analysis and investigation. Future work is directed toward meeting the science objectives that require assessments of boundary layer transition, stagnation point heating, turbulent heating augmentation, surface recession, and in-depth thermal response. Both forward and IPE analysis approaches are being pursued to reconstruct the best estimated aerothermal environment and TPS response. A comprehensive sensitivity analysis is being performed to determine different combinations of possible model choices that reproduce MISP flight data. The inherent uncertainties and biases in MISP data as well as in analysis techniques are being quantified via a variety of techniques such as arc jet testing, sub-scale modeling, Monte-Carlo uncertainty analysis of models, etc.

Finally, via model validation and subsequent advancements, the current aerothermal and TPS design margins, which are based solely on ground test data, will be re-assessed. It is anticipated that margins applied for surface recession, turbulent heating, stagnation point heating will be significantly improved and strongly substantiated.

Acknowledgements

We would like to thank MEDLI and Hypersonics Project Management, especially Alan Little, Michelle Munk, Jim Pittman, and Michael Wright for their support and advocacy for this work. Special thanks are due to Chris Kuhl and Ron Verhappen. We would like to acknowledge the assistance of MSL project staff at Jet Propulsion Laboratory and other NASA centers. This work would not be possible without the help and support from NASA Ames TPS Sensor group led by Ed Martinez, and the personnel at the NASA Ames Arc Jet Complex. Technical input from Karl Edquist, Dinesh Prabhu, Y.K. Chen and Frank Milos are also acknowledged. Finally, we would like to thank Dean Kontinos, Helen Hwang, Ryan McDaniel, and Kerry Zarchi for providing valuable comments to improve this manuscript. Portions of this work are conducted under NASA contract NNA10DE12C to ERC, Incorporated and a NASA grant NNX12AF94A to Georgia Institute of Technology.

References

[1] Steltzner, A.D, et al. “Mars Science Laboratory Entry Descent Landing System Overview,”
[2] Edquist, K.T., Dyakonov, A. A., Wright, M. J., Tang, C.Y., “Aerothermodynamic Design of the Mars Science Laboratory Heatshield,” AIAA Paper No. 2009-4075, Jane 2009.
[3] Wright, M., et. al, "Sizing and Margins Assessment of the Mars Science Laboratory Aeroshell Thermal Protection System" AIAA Paper No. 2009-4231, June 2009.
[4] Beck, R.A.S., et al., “Development of the Mars Science Laboratory Heatshield Thermal Protection System,” AIAA Paper 2009-4229, June 2009.
[5] Drake, B.G. (editor), “Reference Mission Version 3.0 Addendum to the Human Exploration of Mars: The Reference Mission of the NASA Mars Exploration Study Team,” NASA/SP-601-ADD.
[6] Dwyer-Ciancolo, A.M, et al., “Entry Descent and Landing Systems Analysis Study: Phase 2 Report on Exploration Feed-Forward Systems,” NASA/TM-2011-217055, Feb 2011.
[7] Adler, M., Wright, M., Campbell, C., Clark, I., Englund, W., and Rivellini, T., “Entry, Descent, and Landing Roadmap Technology Area 09,” April 2012 (http://www.nasa.gov/pdf/501326main_TA09-ID_rev5_NRC_wTASR.pdf)

[8] Bose, D., Brown, J.L., Prabhu, D., Gnoffo, P., Johnston, C..O., and Hollis, B., "Uncertainty Assessment of Hypersonic Aerothermodynamics Prediction Capability," *(to appear in Journal of Spacecraft and Rockets, 2013)* AIAA Paper 2011-3141, June 2011.
[9] Hollis, B and Prabhu, D., "Assessment of Laminar, Convective Aeroheating prediction Uncertainties for Mars Entry Vehicles," *(to appear in Journal of Spacecraft and Rockets, 2013)* AIAA-2011-3144, June 2011.
[10] Wright, M., Equist, K., Tang, C., Hollis, B., Krasa, P., and Campbell, C., "A Review of Aerothermal Modeling for Mars Entry Missions," AIAA-2010-XXX, January 2010.
[11] Gazarik, M., et al. "Overview of the MEDLI Project," IEEE Paper 2008-1510, March 2008.
[12] Edquist, K.T., Wright, M.J., and Allen, G.A., "Viking Afterbody Heating Computations and Comparisons to Flight Data," AIAA Paper 2006-386, Jan 2006.
[13] Milos, F., Chen, Y,K., Congdon, W., and Thornton, J., "Mars Pathfinder Entry Temperature Data, Aerothermal Heating, and Heatshield Material Response," *Journal of Spacecraft and Rockets*, Vol. 36, No. 3, 1999, pp. 380-391.
[14] Mahzari, M., Braun, R.D., and White, T.R., "Reconstruction of Mars Pathfinder Aerothermal Heating and Heatshield Material Response Using Inverse Methods," AIAA-Paper 2012-2872, Jun 2012.
[15] Bose, D., Skokova, K., Wright, M., and Reuther, J., "Ground-to-Flight Traceability Analysis of Arc Jet Testing for the Crew Exploration Vehicle," AIAA Paper No. 2009-3845, Jun 2009.
[16] MacLean, M., Dufrene, A., and Holden, M., "Spherical Capsule Heating in High Enthalpy Carbon Dioxide in LENS-XX Expansion Tunnel ," AIAA Paper 2013-XXXX, Grapevine, TX, Jan 2013.
[17] Driver, D.M., et al. "Arc Jet Testing in Shear Environment for Mars Science Laboratory Thermal Protection System," AIAA Paper 2009-4230, Jun 2009.
[18] Karlgaard, C.D., Kutty, P., Schoenenberger, M., Schidner,J., and Munk, M., "Mars Entry Atmospheric Data System Trajectory Reconstruction Algorithms and Flight Results," AIAA Paper 2013-XXXX, Grapevine, TX, Jan 2013.
[19] Mahzari, M., Braun, R.D., White, T., Bose, D., "Preliminary Analysis of the Mars Science Laboratory's Entry Aerothermodynamic Environment and Thermal Protection System Performance," AIAA Paper 2013-XXXX, Jan 2013.
[20] Gorbunov S. et al. "Thermal Protection System Ablation Sensor," US Patent 8,069,001 B1, Nov. 29, 2011.
[21] Wright, M. J., Candler, G. V., and Bose, D., "Data-Parallel Line Relaxation Method of the Navier-Stokes Equations," *AIAA Journal*, Vol. 36, No. 9, 1998, pp., 1603-1609.
[22] Milos, F.S. and Chen, Y.K., "Comprehensive Model for Multicomponent Ablation Thermochemistry," AIAA-97-0141, Jan 1997.
[23] Mitcheltree, R.A. and P.A. Gnoffo, "Wake Flow About a MESUR Mars Entry Vehicle," AIAA 94-1958, June 1994.
[24] Santos, J., White, T., and Cozmuta, I., "MSL Entry, Descent, and Landing Instrumentation-MISP Error Budget Report," Document No. MEDLI-0236, Feb 2011.
[25] Santos, J.A., Oishi, T., Martinez, E.R., "Isotherm Sensor Calibration program for Mars Science Laboratory Heat Shield Flight Data Analysis," AIAA 2011-3955, June 2011.
[26] Martinez, E.R., Weber, C.T., Oishi, T., Santos, J., and Mach, J., "Development of a Sheathed Miniature Aerothermal Reentry Thermocouple for Thermal Protection System Materials," AIAA 2011-3321, Jun 2011.
[27] White, T., Cozmuta, I., Santos, J.A., Laub, B., and Mahzari, M., "Proposed Analysis Process for Mars Science Laboratory Heat Shield Sensor Plug Flight Data," AIAA Paper 2011-3957, June 2011.
[28] Hollis, B.R., and Collier, A.S., "Turbulent Aeroheating Testing of Mars Science Laboratory Entry Vehicle," *Journal of Spacecraft and Rockets*, Vol. 45, No. 3, May-Jun. 2008, pp. 417-427.
[29] Reda, D.C., Wilder, M.C., and Prabhu, D.K., Transition Experiments on Blunt Bodies with Isolated Roughness Elements in Hypersonic Flight," *Journal of Spacecraft and Rockets*, Vol. 47, No. 5, Sept.-Oct. 2010, pp. 828-835.
[30] Milos, F., Chen, Y-K., and Gokcen, T., "Non-Equilibrium Ablation of Phenolic Impregnated Carbon Ablator," AIAA Paper 2010-981, Jan 2010.